

A Consensus Equilibrium Solution for Deep Image Prior Powered by Red

Hyder, Rakib; Mansour, Hassan; Ma, Yanting; Boufounos, Petros T.; Wang, Pu

TR2021-046 May 11, 2021

Abstract

Recent advances in solving imaging inverse problems have witnessed the combination of deep learning models with classical image models for better signal representation. One such approach, DeepRED, combines the deep image prior (DIP) with the regularization by denoising (RED) framework to boost the performance of image deblurring and super resolution tasks. In this paper, we formulate DeepRED as a consensus equilibrium problem and set up a fixed-point algorithm for solving the equilibrium equations. We also derive sufficient conditions that the DIP generative prior should satisfy to ensure that the corresponding fixed-point operator is nonexpansive. We then demonstrate that the fixed-point algorithm that solves the CE equations results in improved image reconstruction quality in a deblurring setting compared to state-of-the-art methods

IEEE International Conference on Acoustics, Speech, and Signal Processing (ICASSP)

A CONSENSUS EQUILIBRIUM SOLUTION FOR DEEP IMAGE PRIOR POWERED BY RED

Rakib Hyder^a, Hassan Mansour^b, Yanting Ma^b, Petros T. Boufounos^b, Pu Wang^b

^a Department of Electrical and Computer Engineering, University of California, Riverside, CA 92521

^bMitsubishi Electric Research Laboratories, Cambridge, MA 02139
rhyde001@ucr.edu, {mansour, yma, petrosb, pwang}@merl.com

ABSTRACT

Recent advances in solving imaging inverse problems have witnessed the combination of deep learning models with classical image models for better signal representation. One such approach, DeepRED, combines the deep image prior (DIP) with the regularization by denoising (RED) framework to boost the performance of image deblurring and super resolution tasks. In this paper, we formulate DeepRED as a consensus equilibrium problem and set up a fixed-point algorithm for solving the equilibrium equations. We also derive sufficient conditions that the DIP generative prior should satisfy to ensure that the corresponding fixed-point operator is non-expansive. We then demonstrate that the fixed-point algorithm that solves the CE equations results in improved image reconstruction quality in a deblurring setting compared to state-of-the-art methods.

Index Terms— Inverse problem, image deblurring, consensus equilibrium, deep image prior, RED

1. INTRODUCTION

Image blurring is a common artifact that arises due to a variety of problems during the image capturing stage, such as, motion/shaking of the camera, out-of-focus acquisition, atmospheric aberrations, and low-light conditions. Image deblurring is the task of resolving the blurring artifacts when the source of the blur is known. The problem can be formalized as the task of recovering a true signal \mathbf{x} from blurred measurements \mathbf{y} and given the blurring operator \mathbf{A} , such that,

$$\mathbf{y} = \mathbf{A}\mathbf{x} + \eta, \quad (1)$$

where η is the noise introduced during measurement acquisition process, which is assumed to be additive white Gaussian noise (AWGN). The blurring operator \mathbf{A} convolves a blurring kernel with the true signal in the measurement model.

Image deblurring is an ill-posed problem when the operator \mathbf{A} is rank deficient and in the presence of noise. Therefore, there can be infinitely many solutions \mathbf{x} that satisfy equation (1). A general approach to solving ill-posed problems is to add a regularizer that constrains the solution set to a small subset of the feasible space. We can write a general regularized inverse problem as

$$\min_{\mathbf{x}} \|\mathbf{y} - \mathbf{A}\mathbf{x}\|_2^2 + \lambda\rho(\mathbf{x}), \quad (2)$$

where $\rho(\mathbf{x})$ is the regularizing penalty function, and λ is a regularization parameter. The choice of regularizer is specific to the type of signals \mathbf{x} that are desired. In the case of images, a wide variety of regularizers have been proposed to regularize reconstruction in the denoising setting, i.e., when \mathbf{A} is the identity operator. These

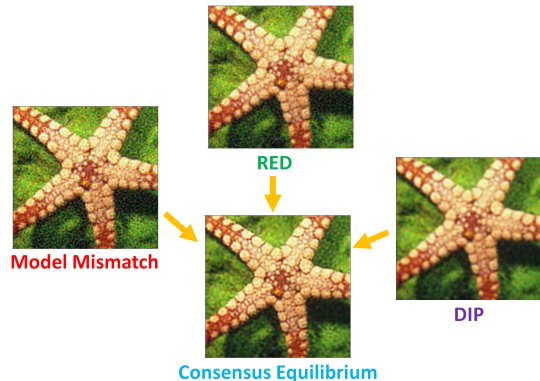


Fig. 1. Consensus Equilibrium of model mismatch, RED, and DIP. The top images result from the action of different agents that are combined to produce the CE solution.

include “classical” prior models [1, 2, 3, 4, 5, 6, 7, 8], and deep learning models [9, 10]. Moreover, sophisticated denoiser models that leverage nonlocal self-similarity in images are popular in state-of-the-art methods, such as, block-matching with 3D transform denoising (BM3D) [2], nonlocal means (NLM) [1], and NCSR [11].

In the context of general inverse problems with rank deficient \mathbf{A} , a relatively new line of work has opted to replace explicit regularizing penalty functions $\rho(\mathbf{x})$ with the deep network-based models or the sophisticated denoisers. Of note, are the plug-and-play (PnP) framework [12], and regularization by denoising (RED) [13]. The PnP framework tackles problem (2) using proximal gradient descent and replaces the proximal mapping with respect to $\rho(\cdot)$ with a signal denoiser $\mathcal{D}(\mathbf{x})$. In a related manner, the RED technique assumes that the regularizing penalty function is given by

$$\rho(\mathbf{x}) = \mathbf{x}^T(\mathbf{x} - \mathcal{D}(\mathbf{x})). \quad (3)$$

Note that the penalty function above is only valid when the denoiser is locally homogeneous with a symmetric Jacobian [14]. Otherwise, RED assumes that $\nabla\rho(\mathbf{x}) = \mathbf{x} - \mathcal{D}(\mathbf{x})$. We will focus in this paper on the RED approach although our formulation also extends to the PnP framework.

In another line of work, untrained convolutional network architectures have been used as image prior. Deep image prior (DIP) [15] and its variants [16, 17] utilize the structural bias of convolutional networks towards producing natural images [18] in fewer update iterations compared to modeling noise. Using $\mathbf{x} = \mathcal{G}(\mathbf{z}, \theta)$ where $\mathcal{G}(\mathbf{z}, \theta)$ is a generator network using latent code, \mathbf{z} and network weights θ , we can write the DIP prior as

$$\min_{\theta} \|\mathbf{y} - \mathbf{A}\mathcal{G}(\theta)\|_2^2. \quad (4)$$

R. Hyder conducted this work during an internship at MERL.

These untrained models, however, are susceptible to modeling measurement noise as well [15, 18] given enough optimization iterations.

In this paper, we focus on an ensemble regularization framework, called DeepRED [19], that combines the RED approach with a nonlocal means denoiser and the deep image prior architecture. We recast the DeepRED problem in the context of Consensus Equilibrium (CE) [20] and specify the set of equilibrium equations for each of the model mismatch function, the RED denoiser, and the DIP denoiser that need to be satisfied by the target reconstructed image, as illustrated in Fig. 1. Contrary to the DeepRED solution that relies on an alternating direction method of multipliers (ADMM) algorithm, we use a fixed-point algorithm to solve the set of equilibrium equations. We demonstrate that the versatility provided by the CE framework leads to improved deblurring image quality compared to DeepRED, especially under high noise and high blurring situations. We also derive sufficient conditions for the generative prior network of DIP to guarantee convergence of the fixed-point iteration.

In the next section, we provide further details on the two related works, namely, DeepRED and consensus equilibrium. We then develop the CE formulation of the DeepRED problem in Section 3 and set up the corresponding fixed-point problem that is solved using the Mann iterations. A sufficient condition that guarantees convergence of the Mann iterations is that the fixed-point operator be nonexpansive. To that end, we derive sufficient conditions on the generative prior that guarantee that the corresponding fixed-point operator is nonexpansive. Finally, we validate the performance of our proposed approach in Section 4 and demonstrate improved reconstruction quality over DeepRED, DIP, RED, and NCSR.

2. RELATED WORK

The deep image prior powered by the RED framework, or DeepRED [19], combines the representation power of the deep image priors with the superior denoising capabilities of a nonlocal means denoiser. [19] proposed an ADMM algorithm for solving the augmented Lagrangian of the DeepRED problem given by:

$$\min_{\theta, \mathbf{x}} \frac{1}{2} \|\mathbf{A}\mathcal{G}(\theta) - \mathbf{y}\|_2^2 + \frac{\lambda}{2} \mathbf{x}^T (\mathbf{x} - \mathcal{D}(\mathbf{x})) + \frac{\mu}{2} \|\mathbf{x} - \mathcal{G}(\theta) - \mathbf{u}\|_2^2 - \frac{1}{2} \|\mathbf{u}\|_2^2, \quad (5)$$

where \mathbf{u} denotes the scaled dual multiplier, and μ is a step size parameter. The above formulation ties the inaccuracies of the measurement process to the rich parameterization of the generative prior. Although this formulation works well for low noise and low blurring scenarios, it suffers in the high noise setting as it tends to overfit the noisy measurements, a behavior that has also been seen in DIP.

Consensus equilibrium [20] presents a multi-agent satisfaction framework that generalizes consensus optimization to cover models and operators that are not associated with explicit optimization problems. The CE framework extends the consensus optimization objective

$$\min_{\mathbf{x}_i, \mathbf{z}} \sum_{i=1}^N \mu_i f_i(\mathbf{x}_i) \text{ s.t. } \mathbf{x}_i = \mathbf{z}, \sum_{i=1}^N \mu_i = 1, \quad (6)$$

to defining a set of N vector-valued maps $F_i : \mathbb{R}^n \rightarrow \mathbb{R}^n$. The CE of these maps is then defined as any solution $(\mathbf{x}^*, \mathbf{u}^*) \in \mathbb{R}^n \times \mathbb{R}^{nN}$ that satisfies the equations

$$F_i(\mathbf{x}^* + \mathbf{u}_i^*) = \mathbf{x}^*, \quad i = 1, \dots, N$$

$$\sum_{i=1}^N \mu_i \mathbf{u}_i^* = 0, \quad (7)$$

where $\mathbf{u}^* := [\mathbf{u}_1^{*T}, \dots, \mathbf{u}_N^{*T}]^T$. In the following sections, we derive the CE equations for the DeepRED problem, setting up the corresponding fixed-point equations, and demonstrating the improved performance over DeepRED's ADMM implementation.

Other recent efforts on the image deblurring have been based on variants of the fast iterative shrinkage/thresholding algorithm (FISTA) [21, 22], and on trained generative prior [23]. While these methods demonstrate state-of-the-art performance on image deblurring, they could be combined with our framework as additional mapping functions in the CE formulation.

3. CONSENSUS EQUILIBRIUM FOR DIP AND RED

In this section, we describe a consensus equilibrium perspective for combining DIP and RED to regularize linear inverse problems.

3.1. DeepRED as fixed-point CE

We begin with a reformulation of the DeepRED objective, which disentangles the parameterization of the generative prior from the measurement process:

$$\min_{\mathbf{x}, \theta} \mu_1 \|\mathbf{y} - \mathbf{A}\mathbf{x}\|_2^2 + \mu_2 \mathbf{x}^T (\mathbf{x} - \mathcal{D}(\mathbf{x})) + \mu_3 \|\mathbf{x} - \mathcal{G}(\theta)\|_2^2. \quad (8)$$

It can be seen from the above formulation that consensus is sought for three objectives:

$$f_1(\mathbf{x}, \theta) = \|\mathbf{y} - \mathbf{A}\mathbf{x}\|_2^2$$

$$f_2(\mathbf{x}, \theta) = \mathbf{x}^T (\mathbf{x} - \mathcal{D}(\mathbf{x}))$$

$$f_3(\mathbf{x}, \theta) = \|\mathbf{x} - \mathcal{G}(\theta)\|_2^2,$$

where the measurement mismatch objective, $f_1(\mathbf{x}, \theta)$, and the RED objective, $f_2(\mathbf{x}, \theta)$, are in fact independent of θ . Following the CE framework, we can now define three *agents* in the form of proximal mappings with respect to each of the objectives f_i as follows:

$$F_1(\mathbf{v}) = \arg \min_{\mathbf{x}} \|\mathbf{y} - \mathbf{A}\mathbf{x}\|_2^2 + \frac{1}{2\sigma^2} \|\mathbf{v} - \mathbf{x}\|_2^2$$

$$F_2(\mathbf{v}) = \arg \min_{\mathbf{x}} \|\mathbf{x}^T (\mathbf{x} - \mathcal{D}(\mathbf{x}))\|_2^2 + \frac{1}{2\sigma^2} \|\mathbf{v} - \mathbf{x}\|_2^2$$

$$F_3(\mathbf{v}, \theta) = \arg \min_{\mathbf{x}, \phi} \|\mathbf{x} - \mathcal{G}(\phi)\|_2^2 + \frac{1}{2\sigma^2} (\|\mathbf{v} - \mathbf{x}\|_2^2 + \|\phi - \theta\|_2^2) \quad (9)$$

Consensus equilibrium for these agents is defined as in (7), where the variables \mathbf{u}_i are slack variables that relate to the dual multipliers in the consensus optimization setting.

The evaluation of F_1 and F_2 is relatively straightforward and is given by the following equations

$$F_1(\mathbf{v}_1) = \left(\mathbf{A}^T \mathbf{A} + \frac{1}{2\sigma^2} \mathbf{I} \right)^{-1} \left(\mathbf{A}^T \mathbf{y} + \frac{\mathbf{v}_1}{2\sigma^2} \right)$$

$$F_2(\mathbf{v}_2) = \frac{2\sigma^2 \mathcal{D}(\mathbf{v}_2) + \mathbf{v}_2}{2\sigma^2 + 1}$$

The DIP agent, on the other hand, is a function of both the signal \mathbf{x} and the generative prior parameters ϕ . Its evaluation can be performed sequentially by first computing ϕ^* , followed by the update for \mathbf{v}_3 using the following equations:

$$\phi^* = \arg \min_{\phi} \|\mathbf{v}_3 - \mathcal{G}(\phi)\|_2^2 + \frac{2\sigma^2 + 1}{2\sigma^2} \|\phi - \theta\|_2^2$$

$$F_3(\mathbf{v}_3) = \frac{\mathbf{v}_3}{2\sigma^2 + 1} + \frac{2\sigma^2}{2\sigma^2 + 1} \mathcal{G}(\phi^*) \quad (11)$$

Algorithm	Gaussian Kernel ($\sigma_k = 1.6$)					Uniform Kernel				
	Butterfly	Leaves	Parrots	Starfish	Average	Butterfly	Leaves	Parrots	Starfish	Average
CE-DIP+RED	32.27	32.76	33.34	33.09	32.87	31.31	31.32	32.32	31.1	31.55
DeepRED	32.19	32.27	32.84	32.74	32.51	31.44	31.21	32.03	31.06	31.43
DIP	31.21	31.51	31.91	31.83	31.62	30.26	30.38	31.00	30.42	30.51
RED	31.66	31.93	33.33	32.49	32.35	30.41	30.13	31.83	30.57	30.74
NCSR Deblur	30.84	31.57	33.39	32.27	32.02	29.68	29.98	31.95	30.28	30.47
Blurred	22.81	22.12	26.96	25.83	24.43	19.07	18.28	23.87	22.56	20.94

Table 1. Comparison of reconstruction PSNR among the different algorithms under low noise setting ($\sigma_n = \sqrt{2}/255$).

Notice that with the evaluation of ϕ^* in (11), we solve for a regularized set of generative prior parameters. This additional regularization helps in limiting the noise overfitting behavior that is generally observed with DIP. The regularization also relaxes the dependence on the heuristic of assigning an arbitrary number of iterations while updating ϕ to limit the noise overfitting.

As in [20], we reformulate CE as a fixed-point problem. Denoting $\mathbf{v}_i = \mathbf{x} + \mathbf{u}_i$, we have $\mathbf{v}_\mu := \sum_i \mathbf{v}_i = \mathbf{x}$. Further with $F(\mathbf{v}) = [F_1(\mathbf{v}_1)^T, F_2(\mathbf{v}_2)^T, F_3(\mathbf{v}_3)^T]^T$ and $H_\mu(\mathbf{v}) = [\mathbf{v}_\mu^T, \mathbf{v}_\mu^T, \mathbf{v}_\mu^T]^T$, where $\mathbf{v} = [\mathbf{v}_1^T, \mathbf{v}_2^T, \mathbf{v}_3^T]^T$, the CE equations are rewritten as:

$$F(\mathbf{v}) = H_\mu(\mathbf{v}). \quad (12)$$

Due to the linearity of H_μ , we can use Corollary 3 of [20] to define the following equivalent fixed-point problem:

$$(2H_\mu - \mathbf{I})(2F - \mathbf{I})(\mathbf{v}) = \mathbf{v}, \quad (13)$$

where \mathbf{I} is the identity operator.

Next, define the operator $T := (2H_\mu - \mathbf{I})(2F - \mathbf{I})$. When T is nonexpansive and has a fixed-point, the Mann iteration can be used to solve for the fixed-point of (13) as follows:

$$\mathbf{v}^{k+1} = (1 - \rho^k)\mathbf{v}^k + \rho^k T(\mathbf{v}^k), \quad (14)$$

where $\rho^k \in (0, 1)$ is a step size parameter. Theorem 5.15 in [24] shows that when T is nonexpansive, a step size sequence that obeys $\sum_{k \in K} \rho_k(1 - \rho_k) = +\infty$ allows (14) to converge weakly to a point in the fixed-point set of T . Examples of such sequence are the constant step size $\rho_k = \rho \forall k$, and the p-series, $\rho_{k+1} = \rho_k k^{-c}$ for $0 < c < 1$, which enjoys faster convergence.

3.2. On the nonexpansiveness of $(2F_3 - \mathbf{I})$

The regularization of the generative prior parameters in (11) helps in specifying sufficient conditions for ensuring that the operator $(2F_3 - \mathbf{I})$ is nonexpansive. Proposition 1 summarizes this result, but we exclude the proof due to space limitations.

Proposition 1. *Suppose that $\mathcal{G}(\phi)$ is differentiable and L -Lipschitz. Let $J_{\mathcal{G}}(\phi) = \nabla_{\phi} \mathcal{G}(\phi)$ denote the Jacobian matrix of \mathcal{G} evaluated at ϕ and let $\phi_{\mathbf{v}}^* = \arg \min_{\phi} \|\mathbf{v} - \mathcal{G}(\phi)\|_2^2 + \lambda \|\phi\|_2^2$. If*

$$\begin{aligned} \|J_{\mathcal{G}}(\phi)\|_{op} &\leq \tau, \quad \forall \phi \\ \|J_{\mathcal{G}}(\phi_1) - J_{\mathcal{G}}(\phi_2)\|_{op} &\leq L' \|\phi_1 - \phi_2\|_2, \quad \forall \phi_1, \phi_2 \\ \|\mathbf{v} - \mathcal{G}(\phi_{\mathbf{v}}^*)\|_2 &\leq B, \quad \forall \mathbf{v} \end{aligned} \quad (15)$$

and choose λ such that $\lambda \geq 2L\tau + L'B$, then the operator $2F_3 - \mathbf{I}$ is nonexpansive.

(σ_k, σ_n)	Algorithms	Butterfly	Leaves	Parrots	Starfish	Average
(1.6, $\frac{8}{255}$)	CE	28.59	28.79	30.66	29.63	29.42
	DeepRED (2000 iters)	28.69	28.23	30.1	28.71	28.93
	DeepRED (20000 iters)	22.47	24.1	22.81	22.59	23
	Blurred	22.55	21.89	26.34	25.32	24.02
(1.6, $\frac{32}{255}$)	CE	24.32	24.34	27.19	25.42	25.32
	DeepRED (250 iters)	25.18	23.83	27.02	25.1	25.28
	DeepRED (1000 iters)	22	22.12	23.64	21.99	22.44
(2.4, $\frac{\sqrt{2}}{255}$)	Blurred	19.9	19.64	21.59	21.21	20.58
	CE	28.33	27.93	30.43	29.39	29.02
	DeepRED	22.12	21.37	26.41	25.2	23.78
(3.2, $\frac{\sqrt{2}}{255}$)	Blurred	20.29	19.54	24.94	23.66	22.11
	CE	25.62	24.4	28.1	27.21	26.33
	DeepRED	19.47	18.76	24.4	23	21.41
	Blurred	18.69	18.03	23.85	22.36	20.73

Table 2. Comparison of reconstruction PSNR for different noise levels and blurring kernel strengths.

4. EXPERIMENTAL VALIDATION

We follow an experimental setup similar to the that developed in [19], [13] and [25]. Given a blurred and noisy image with a known degradation operator, the goal is to recover the sharp and noise-free original image. We consider blurring kernels with varying blurring effect controlled by the parameter σ_k and add varying levels of i.i.d. Gaussian noise with variance σ_n .

To evaluate the reconstruction, we used four images from the NCSR dataset [11] (Butterfly, Leaves, Parrot and Starfish) similar to the selection in [19]. Each of these images has 256×256 pixels with RGB color channels. For fair comparison with [19], we also use the same nonlocal means (NLM) denoiser.

In the first set of experiments, we replicate the evaluation setup from [19]. Two blurring kernels are used; one kernel is a 9×9 pixel uniform blur, and the other is a 25×25 pixel Gaussian blur of variance $\sigma_k = 1.6$. For both blurring cases, the measurement noise variance is set equal $\sigma_n = \sqrt{2}/255$. The deblurring results are shown in Table 1 which lists the reconstructed peak signal to noise ratio (PSNR) values for the different deblurring algorithms, namely, DeepRED [19], DIP [15], RED [13] and NCSR Deblur [11]. Notice that our proposed CE-based solution (CE-DIP+RED) achieves the best performance in almost all cases, resulting in an average improvement over DeepRED of 0.36dB in PSNR for the Gaussian blurring case and 0.12dB in the uniform blurring case. We can also observe that for this experimental regime, DeepRED performs nearly as well as CE-DIP+RED and outperforms the other three competing methods.

The above experiment is considered a low-noise and low-blur regime. For a more extensive evaluation, we test the performance of CE-DIP+RED and compare it to DeepRED under higher noise and blurring regimes. The results are reported in Table 2. We can observe

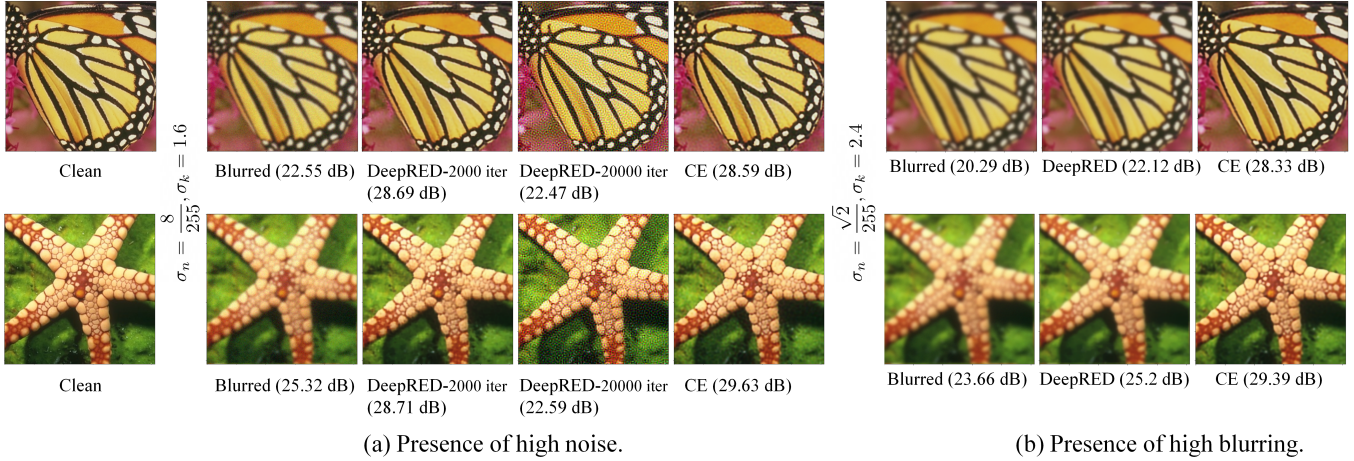


Fig. 2. Image deblurring performance of DeepRED and CE formulation under (a) the presence of high noise ($\sigma_n = 8/255, \sigma_k = 1.6$) and (b) the presence of high blurring ($\sigma_n = \sqrt{2}/255, \sigma_k = 2.4$).

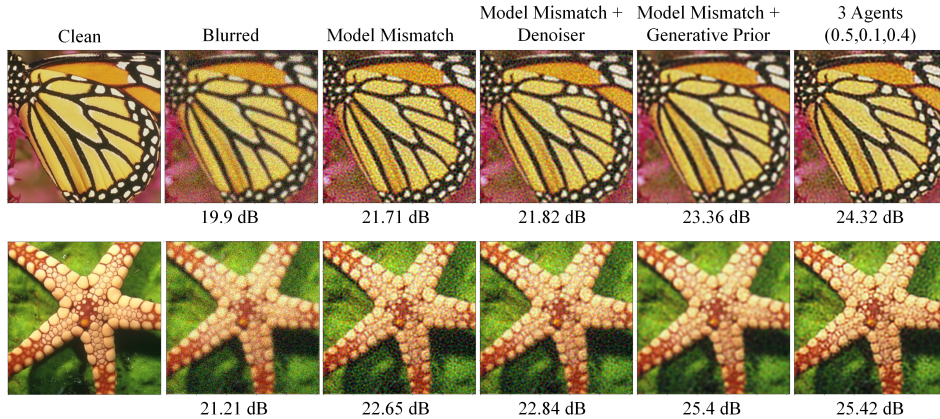


Fig. 3. Reconstruction quality resulting from the combination of the three different agents.

Weights on Agents (Mismatch, RED, DIP)	Butterfly	Leaves	Parrots	Starfish	Average
Mismatch (1,0,0)	21.71	21.85	22.98	22.65	22.3
Mismatch + RED (0.5,0.5,0)	21.82	21.92	23.19	22.84	22.44
Mismatch + DIP (0.5,0,0.5)	23.36	22.54	26.56	25.4	24.46
Mismatch + RED + DIP (0.5,0.1,0.4)	24.32	24.34	27.19	25.42	25.32
Blurred	19.9	19.64	21.59	21.21	20.58

Table 3. Reconstruction PSNR for the different agents.

that under the higher noise condition, the performance of DeepRED is less stable in that it achieve a high PSNR in early iterations but converges to a solution with much lower PSNR. This behavior is consistent with the analysis from [18] and [15] and is most likely a result of the deep image prior overfitting the noise in the measurements. On the other hand, our CE-DIP+RED does achieves a higher reconstruction PSNR at convergence and does not succumb to the

noise overfitting problem. A qualitative evaluation is also shown for *medium* noisy measurements regime ($\sigma_n = 8/255$) in Figure 2. In the case of large blurring artifacts, Table 2, also shows that our CE-DIP+RED significantly outperforms DeepRED. Qualitative results are also shown for *medium* blurred images ($\sigma_k = 2.4$) in Figure 2. Finally, we conduct an ablation study to realize the effect of each of the different agents on the reconstruction quality. For these experiments, we used a Gaussian kernel with $\sigma_k = 1.6$ and measurement noise variance $\sigma_n = 32/255$. Table 3 shows the reconstruction PSNR and demonstrates that the combination of all three agents results in the best reconstruction performance. Moreover, the table shows that benefit of the generative prior over the NLM denoiser. A qualitative comparison is also shown in Figure 3.

5. CONCLUSION

In conclusion, we demonstrated that the CE framework provides a more versatile and robust algorithmic approach for combining multiple signal priors in the inverse problem setting compared to ADMM. We also presented sufficient conditions on the generative prior of DIP that guarantee the nonexpansive property of the corresponding fixed-point operator.

6. REFERENCES

- [1] Antoni Buades, Bartomeu Coll, and J-M Morel, "A non-local algorithm for image denoising," in *2005 IEEE Computer Society Conference on Computer Vision and Pattern Recognition (CVPR'05)*. IEEE, 2005, vol. 2, pp. 60–65.
- [2] Kostadin Dabov, Alessandro Foi, Vladimir Katkovnik, and Karen Egiazarian, "Image denoising by sparse 3-d transform-domain collaborative filtering," *IEEE Transactions on image processing*, vol. 16, no. 8, pp. 2080–2095, 2007.
- [3] Julien Mairal, Francis Bach, Jean Ponce, Guillermo Sapiro, and Andrew Zisserman, "Non-local sparse models for image restoration," in *2009 IEEE 12th international conference on computer vision*. IEEE, 2009, pp. 2272–2279.
- [4] Michael Elad and Michal Aharon, "Image denoising via sparse and redundant representations over learned dictionaries," *IEEE Transactions on Image processing*, vol. 15, no. 12, pp. 3736–3745, 2006.
- [5] Leonid I Rudin, Stanley Osher, and Emad Fatemi, "Nonlinear total variation based noise removal algorithms," *Physica D: nonlinear phenomena*, vol. 60, no. 1-4, pp. 259–268, 1992.
- [6] Stanley Osher, Martin Burger, Donald Goldfarb, Jinjun Xu, and Wotao Yin, "An iterative regularization method for total variation-based image restoration," *Multiscale Modeling & Simulation*, vol. 4, no. 2, pp. 460–489, 2005.
- [7] Yair Weiss and William T Freeman, "What makes a good model of natural images?," in *2007 IEEE Conference on Computer Vision and Pattern Recognition*. IEEE, 2007, pp. 1–8.
- [8] Xiangyang Lan, Stefan Roth, Daniel Huttenlocher, and Michael J Black, "Efficient belief propagation with learned higher-order markov random fields," in *European conference on computer vision*. Springer, 2006, pp. 269–282.
- [9] Kai Zhang, Wangmeng Zuo, Yunjin Chen, Deyu Meng, and Lei Zhang, "Beyond a gaussian denoiser: Residual learning of deep cnn for image denoising," *IEEE Transactions on Image Processing*, vol. 26, no. 7, pp. 3142–3155, 2017.
- [10] Dong Yang and Jian Sun, "Bm3d-net: A convolutional neural network for transform-domain collaborative filtering," *IEEE Signal Processing Letters*, vol. 25, no. 1, pp. 55–59, 2017.
- [11] Weisheng Dong, Lei Zhang, Guangming Shi, and Xin Li, "Nonlocally centralized sparse representation for image restoration," *IEEE transactions on Image Processing*, vol. 22, no. 4, pp. 1620–1630, 2012.
- [12] Singanallur V Venkatakrishnan, Charles A Bouman, and Brendt Wohlberg, "Plug-and-play priors for model based reconstruction," in *2013 IEEE Global Conference on Signal and Information Processing*. IEEE, 2013, pp. 945–948.
- [13] Yaniv Romano, Michael Elad, and Peyman Milanfar, "The little engine that could: Regularization by denoising (red)," *SIAM Journal on Imaging Sciences*, vol. 10, no. 4, pp. 1804–1844, 2017.
- [14] E. T. Reehorst and P. Schniter, "Regularization by denoising: Clarifications and new interpretations," *IEEE Transactions on Computational Imaging*, vol. 5, no. 1, pp. 52–67, 2019.
- [15] Dmitry Ulyanov, Andrea Vedaldi, and Victor Lempitsky, "Deep image prior," in *Proceedings of the IEEE Conference on Computer Vision and Pattern Recognition*, 2018, pp. 9446–9454.
- [16] Reinhard Heckel and Paul Hand, "Deep decoder: Concise image representations from untrained non-convolutional networks," in *International Conference on Learning Representations*, 2018.
- [17] Rakib Hyder and M Salman Asif, "Generative models for low-dimensional video representation and reconstruction," *IEEE Transactions on Signal Processing*, vol. 68, pp. 1688–1701, 2020.
- [18] Reinhard Heckel and Mahdi Soltanolkotabi, "Denoising and regularization via exploiting the structural bias of convolutional generators," in *International Conference on Learning Representations*, 2019.
- [19] Gary Mataev, Peyman Milanfar, and Michael Elad, "Deepred: Deep image prior powered by red," in *Proceedings of the IEEE International Conference on Computer Vision Workshops*, 2019, pp. 0–0.
- [20] Gregory T Buzzard, Stanley H Chan, Suhas Sreehari, and Charles A Bouman, "Plug-and-play unplugged: Optimization-free reconstruction using consensus equilibrium," *SIAM Journal on Imaging Sciences*, vol. 11, no. 3, pp. 2001–2020, 2018.
- [21] Md Zulfiqar Ali Bhotto, M Omaid Ahmad, and MNS Swamy, "An improved fast iterative shrinkage thresholding algorithm for image deblurring," *SIAM journal on imaging sciences*, vol. 8, no. 3, pp. 1640–1657, 2015.
- [22] Praveen Kumar Pokala and Chandra Sekhar Seelamantula, "Projected improved fista and application to image deblurring," in *2020 IEEE International Conference on Image Processing (ICIP)*. IEEE, 2020, pp. 1043–1047.
- [23] Ashish Bora, Ajil Jalal, Eric Price, and Alexandros G Dimakis, "Compressed sensing using generative models," in *International Conference on Machine Learning*, 2017, pp. 537–546.
- [24] Heinz H Bauschke, Patrick L Combettes, et al., *Convex analysis and monotone operator theory in Hilbert spaces*, vol. 408, Springer, 2011.
- [25] Noam Yair and Tomer Michaeli, "Multi-scale weighted nuclear norm image restoration," in *Proceedings of the IEEE Conference on Computer Vision and Pattern Recognition*, 2018, pp. 3165–3174.